Computers and Geotechnics 150 (2022) 104890

Contents lists available at ScienceDirect

Computers and Geotechnics

journal homepage: www.elsevier.com/locate/compgeo

How can the effect of particle surface roughness on the contact area be predicted?

Sadegh Nadimi [a,*], Vasileios Angelidakis [a], Masahide Otsubo [b], Ali Ghanbarzadeh [c]

[a] School of Engineering, Newcastle University, UK
[b] Institute of Industrial Science, The University of Tokyo, Japan
[c] School of Mechanical Engineering, University of Leeds, UK

ARTICLE INFO

Keywords:
Particle-scale behaviour
Surface roughness
Contact law
Friction

ABSTRACT

This paper describes a systematic study of the effect of fractal rough surfaces on the contact area with the aim of advancing contact constitutive laws used in the Discrete Element Method. An in-house Boundary Element code is adopted to investigate the mechanical behaviour of computer-generated surface roughness. Surfaces are generated to have methodically controlled root mean square height (S_q), root mean square gradient (S_{dq}), short wavevector (q_0), large wavevector (q_1), Hurst exponent (H) and fractal dimension (D_f). The effect of each parameter on the contact area is investigated. Two recently proposed analytical solutions in tribology (*i.e.* Persson-Tosatti and Pastewka-Robbins) are applied to predict the real contact area. A parameter based on S_q, q_0, and H is proposed and its sensitivity for real contact area prediction is demonstrated. Surfaces of natural sand are simulated and their mechanical response shows similar trend as the computer-generated surfaces, albeit more complex.

1. Background

When two real surfaces come into contact, a very small proportion of the nominal contact area will physically sustain the load, known as the real contact area. The real contact area is an important physical quantity since it is known to be responsible for a large number of tribological phenomena such as friction, wear, adhesion, material transformations, chemical reactions, electrical contact resistance *etc*. The importance of contact area is well-accepted in areas such as nano-technology (Ma et al., 2005; Sun et al., 2018), powder technology (Moreno-Atanasio et al., 2007; Wilson et al., 2017), biomedical engineering (Landolt et al., 2001; Ghanbarzadeh et al., 2019), transport (Persson, 2001; Magel and Kalousek, 2002), rock mechanics (Xiao, et al., 2016) and soil mechanics (Santamarina and Cascante, 1998; Yimsiri and Soga, 2000; Otsubo et al., 2015; Yang et al., 2016; Otsubo and O'Sullivan, 2018; Nadimi et al., 2019a; Nadimi et al., 2019b; Wong and Coop, 2020; Yao, et al., 2021; Zhang et al., 2021; Yang et al., 2022).

In geotechnical engineering, the overall behaviour of soils is highly dependent on the interaction of particles with each other. These particle-to-particle interactions are highly influenced by particle characteristics such as their mechanical, mineralogical, and topographical properties. It is therefore important to accurately analyse the interfacial contact mechanics of two particles to be able to predict the overall behaviour of a soil. Hanaor et al. (2013) investigated the evolution of surface roughness using a rough aluminium surface. They found that the number of asperities in contact plays a significant role in the development of surface structure and resultant frictional force. In their subsequent contribution, Hanaor et al. (2016) proposed a roughness modelling approach for the prediction of static friction between rough-to-rough surfaces. Their model facilitates an understanding of how molecular scale friction and adhesive interactions contribute to the development of frictional forces. In an experimental study, Sandeep et al. (2018) reported the frictional response of silica sand grains. They demonstrated that different geological environments cause a variety of particle roughness and form which can be directly correlated to frictional forces. Sandeep et al. (2021) quantified the effect of roughness on both friction and contact stiffness. They observed that the increase in surface roughness significantly reduces the normal stiffness.

Otsubo et al. (2017) proposed a semi-analytical model that takes into account the effect of surface roughness, characterised by the root mean square height (S_q) in the normal force–displacement behaviour of particle interaction. They provided the mathematical expression to model rough contact behaviour considering three regions of force–displacement response, including (i) asperity-dominated (Eq. (1)), (ii) transitional (Eq. (2)), and (iii) equivalent Hertzian contact (Eq. (3)) where the

* Corresponding author.
E-mail address: sadegh.nadimi-shahraki@ncl.ac.uk (S. Nadimi).

https://doi.org/10.1016/j.compgeo.2022.104890
Received 30 January 2022; Received in revised form 30 May 2022; Accepted 25 June 2022
Available online 12 July 2022
0266-352X/© 2022 The Author(s). Published by Elsevier Ltd. This is an open access article under the CC BY license (http://creativecommons.org/licenses/by/4.0/).

Nomenclature

a_0	radius of the nominal contact area
A_c	area of contact
D_f	fractal dimension
E	Young's modulus
E^*	equivalent contact elastic modulus
F_N	load in the normal direction
H	Hurst exponent
H^*	hardness
L	length of the surface in each dimension
$L(F_N)$	limit breakage condition of the breakage model of Zhang et al. (2021)
n_1, n_2	fitting coefficients of the breakage model of Zhang et al. (2021)
N	total number of nodes in the domain
$p(s_1, s_2)$	applied contact pressure
q_0	short wavevector
q_1	large wavevector
r	rigid body movement of two rough surfaces in the normal direction
R	radius of sphere
(s_1, s_2)	coordinate of area that pressure is applied
S_q	root mean squared height
$S_q{}^*$	equivalent root mean squared height
S_{dq}	root mean square gradient
$\overline{u_z}$(x,y)	surface deformations at the interfaces
(x, y)	coordinate in which surface deformation is obtained
Z_1, Z_2	the surface profiles of the two rough particles
α, β	roughness parameters
φ	coefficient of friction
λ_r	roll-off wavelength
λ_s	short wavelength cut-off
ν	Poisson's ratio
ξ, η	coordinates at which the load is applied
σ_{lim}	limit strength of material in the breakage model of Zhang et al (2021)

region shifts with the overlap (δ) of the two surfaces relative to S_q.

$$F_N = N_{GT}\left(\frac{\delta}{2.11S_q}\right)^{2.59} \quad \delta < 2.11S_q \tag{1}$$

$$F_N = \frac{N_{GT}}{100}\left(\frac{\delta - 0.82S_q}{23.65S_q}\right)^{1.58} \quad 2.11S_q \le \delta < 24.47S_q \tag{2}$$

$$F_N = \frac{4}{3}E^* R^{*0.5}\left(\delta - 2.06S_q\right)^{1.5} \quad 24.47S_q \le \delta \tag{3}$$

where E^* is the equivalent contact stiffness given by $\frac{1}{E^*} = \frac{1-\nu_1^2}{E_1} + \frac{1-\nu_2^2}{E_2}$, where E_1 and E_2 are the Young's moduli of the two contacting spheres, ν_1 and ν_2 are the Poisson's ratios of the two contacting spheres; $\frac{1}{R^*} = \frac{1}{R_1} + \frac{1}{R_2}$ and R_1 and R_2 are the radii of the contacting spheres. N_{GT} is the threshold normal force based on the Greenwood and Tripp (1967) assumption, as considered in Cavarretta et al. (2010), so that rough surface contact responses can be described by the Hertzian theory if the normal load exceeds this threshold (Eq. (4)):

$$N_{GT} = 100\sqrt{2}E^* R^{*0.5} S_q^{1.5} \tag{4}$$

It is noteworthy that the investigation of Cavarretta et al. (2010) is based on single-grain tests rather than grain-to-grain contacts. Otsubo et al. (2017) incorporated this formulation in Discrete Element Method (DEM) simulations, which they used to predict the small-strain shear modulus and the dynamic response of granular soils.

Nadimi et al. (2019b) have used a deterministic contact mechanics model informed by the Boundary Element Method (BEM) and developed a semi-analytical model of normal load–displacement for the contact of real rough surfaces (Eq. (5)). The advantage of this model is that it can predict three regions of asperity-dominated, transitional and equivalent Hertzian contact by a single equation, and so it is computationally less expensive.

$$F_N = \frac{4}{3}E^*\sqrt{R^*}\delta^{\left(\frac{3}{2}\right)} - \beta S_q^* E^* \sqrt{R^* S_q^*}\,\mathrm{erf}\left(\alpha\frac{\delta}{S_q^*}\right) \qquad F_N \ge 0 \tag{5}$$

where α and β are the fitting parameters based on BEM prediction and S_q^* is the equivalent root mean height of two contacting surfaces defined as $S_q^* = \sqrt{S_{q1}^2 + S_{q2}^2}$. They implemented Eq. (5) in a commercial DEM code to simulate the interaction of millions of rough particles. The model used a real surface topography as a digitised surface input in the BEM.

Since the explicit incorporation of real rough surfaces in DEM simulations is costly, Mollon et al. (2020) investigated an indirect introduction of roughness in the multi-scale analysis of granular materials, by modifying the interparticle friction coefficient. They concluded that such an assumption is possible to a certain extent and provided guidelines on how roughness can be compensated by friction. Feng et al. (2017) proposed a stochastic discrete element modelling framework for particles with surface roughness. They developed a normal contact interaction law based on the Greenwood and Williamson model, limited to spherical particles. A comparison of statistical micro-contact models based on the classic Greenwood and Williamson model (1966) is provided in Beheshti and Khonsari (2012). More recently, Zhang et al. (2021) expanded the formulations proposed in Otsubo et al. (2017) to breakable particles. They provided three equations for each contact regime to limit the contact normal force acting on a particle. Limiting breakage in the asperity-dominated regime, when $F_N < F_{NT1}$, is expressed by a limit breakage condition $L(F_N)$:

$$L(F_N) = F_N - \sigma_{lim}\pi R^*\left(\frac{F_N}{S_q E^*\sqrt{2R^* S_q}}\right)^{\frac{1}{c}}\left\{\left(\frac{1}{100}\right)^{\frac{1}{b}}\left[\left(\frac{300S_q E^*\sqrt{2R^* S_q}}{4E^*\sqrt{R^*}}\right)^{\frac{2}{3}} + n_2 S_q\right] + n_1 S_q\right\} \tag{6}$$

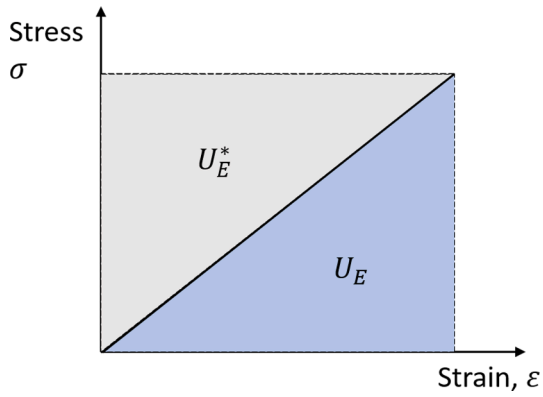


Fig. 1. Relation between U_E^* and U_E for contact between linear elastic materials without plastic deformation.

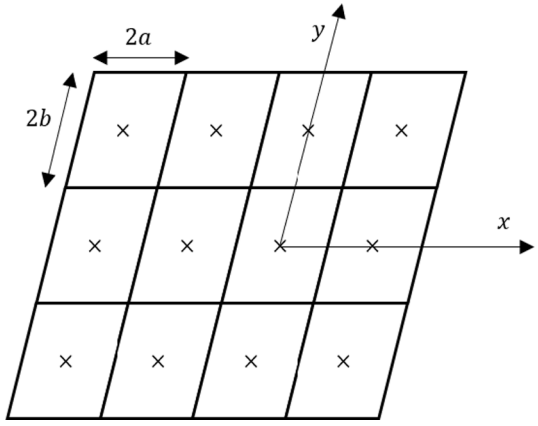


Fig. 2. Discretised elements: ' × ' is the centroid of each element, and 2***a*** and 2***b*** are the side lengths of each element in x and y directions respectively.

In the transitional regime, when $F_{NT1} < F_N < F_{NT2}$

$$L(F_N) = F_N - \sigma_{lim}\pi R^* \left\{ \left(\frac{F_N}{100 S_q E^* \sqrt{2R^* S_q}} \right)^{\frac{1}{b}} \left[\left(\frac{300 S_q E^* \sqrt{2R^* S_q}}{4E^* \sqrt{R^*}} \right)^{\frac{2}{3}} + n_2 S_q \right] + n_1 S_q \right\} \leq 0 \tag{7}$$

and in the Hertzian regime, when $F_{NT2} < F_N$

$$L(F_N) = F_N - \sigma_{lim}\pi R^* \left\{ \left(\frac{9 {F_N}^2}{16 {E^*}^2 R^*} \right)^{\frac{1}{3}} + n_2 S_q + n_1 S_q \right\} \leq 0 \tag{8}$$

where σ_{lim} is the limit strength of the material, and n_1 and n_2 are fitting coefficients. They have incorporated the contact model in a commercial DEM code to predict the effect of contact roughness on single particle breakage.

In Eqs. (1) to (8), the surface roughness is only characterised by one parameter, *i.e.* S_q. However, in tribology, there have been tremendous efforts in developing accurate deterministic contact mechanics models that can accommodate topographical features. Different approaches and the discussion of their capabilities as well as their shortcomings are summarised in a comprehensive paper by Müser et al. (2017). Pastewka

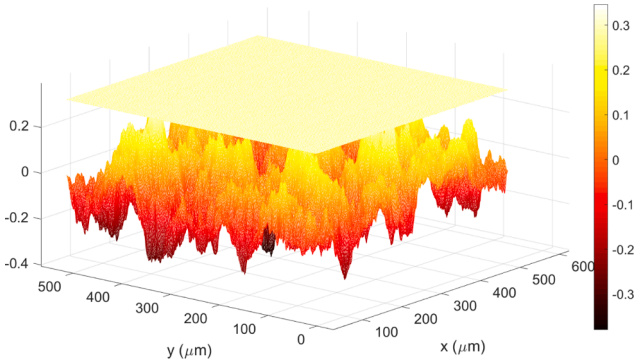


Fig. 4. Schematics of a typical rough surface contact used in this study, the colour map shows the elevation in μm measuring from the average height of the rough surface.

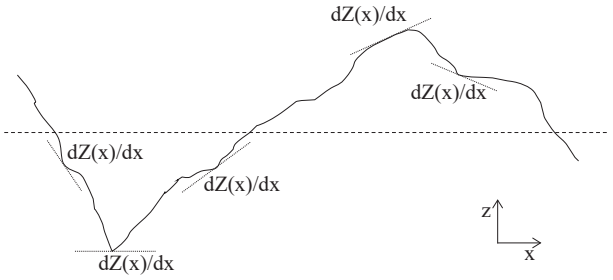


Fig. 5. Schematic representation of the root mean square slope (S_{dq}) within a sampling profile.

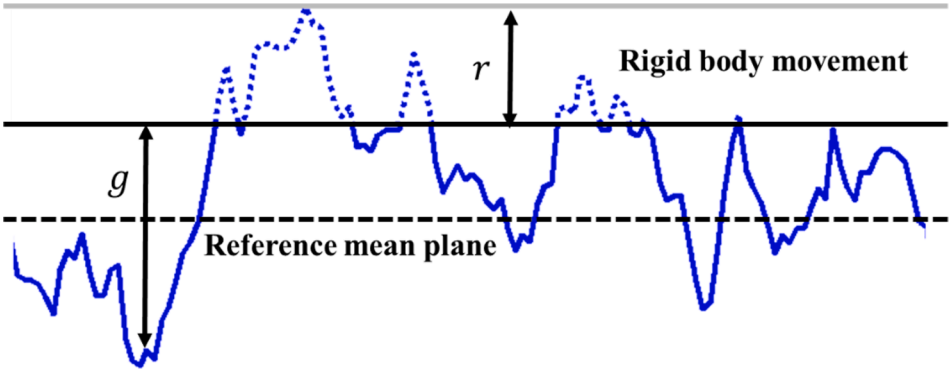


Fig. 3. Schematic of rough surface (blue line) with smooth surface (solid black line) demonstrating the rigid body movement of the smooth profile and the reference mean plane of the rough profile (dashed black line). (For interpretation of the references to colour in this figure legend, the reader is referred to the web version of this article.)

Table 1
Summary of surface parameters used in this study.

Surface	S_q (μm)	S_{dq} (-)	q_0 (m^{-1})	H	q_1 (m^{-1})
Surf 1	0.1	0.0038	$2\pi \times 10^4$	0.8	$5.12\pi \times 10^4$
Surf 2	0.1	0.0106	$8\pi \times 10^4$	0.8	$5.12\pi \times 10^4$
Surf 3	0.1	0.0294	$32\pi \times 10^4$	0.8	$5.12\pi \times 10^4$
Surf 4	0.1	0.1067	$256\pi \times 10^4$	0.8	$5.12\pi \times 10^4$
Surf 5	0.1	0.0169	$8\pi \times 10^4$	0.6	$5.12\pi \times 10^4$
Surf 6	0.1	0.0072	$8\pi \times 10^4$	1	$5.12\pi \times 10^4$
Surf 7	0.1	0.0055	$8\pi \times 10^4$	1.2	$5.12\pi \times 10^4$
Surf 8	0.5	0.0532	$8\pi \times 10^4$	0.8	$5.12\pi \times 10^4$
Surf 9	1	0.1119	$8\pi \times 10^4$	0.8	$5.12\pi \times 10^4$
Surf 10	5	0.5669	$8\pi \times 10^4$	0.8	$5.12\pi \times 10^4$
Surf 11	0.1	0.0482	$8\pi \times 10^4$	0.8	$0.64\pi \times 10^4$
Surf 12	0.1	0.0063	$8\pi \times 10^4$	0.8	$10.24\pi \times 10^4$

and Robbins (2016) proposed a formula for predicting the real contact area for non-adhesive contact of rough surfaces using a mean-field approximation. They showed that small scale roughness parameters such as the root mean square gradient of roughness (S_{dq}) can sufficiently describe the area of contact. Later, Müser (2016a) used their theory to develop a more robust solution, by eliminating the mean-field approximation. He then compared the analytical results with numerical simulations of Green's Function Molecular Dynamics (GFMD). In parallel, a group of researchers investigated different theories such as Persson-Tosatti and Bearing Area Model (BAM) to study the stickiness criteria for rough surfaces (Afferrante et al., 2015; Ciavarella and Papangelo, 2018; Ciavarella, 2020). They have shown that a short wavevector cut-off of surface roughness ($q_0 = \frac{2\pi}{\lambda_r}$ where λ_r is the roll-off wavelength) and S_q are controlling parameters that influence the contact area. There is still an ongoing debate in the community on the influence of characteristics of surface roughness on the prediction of real contact area,

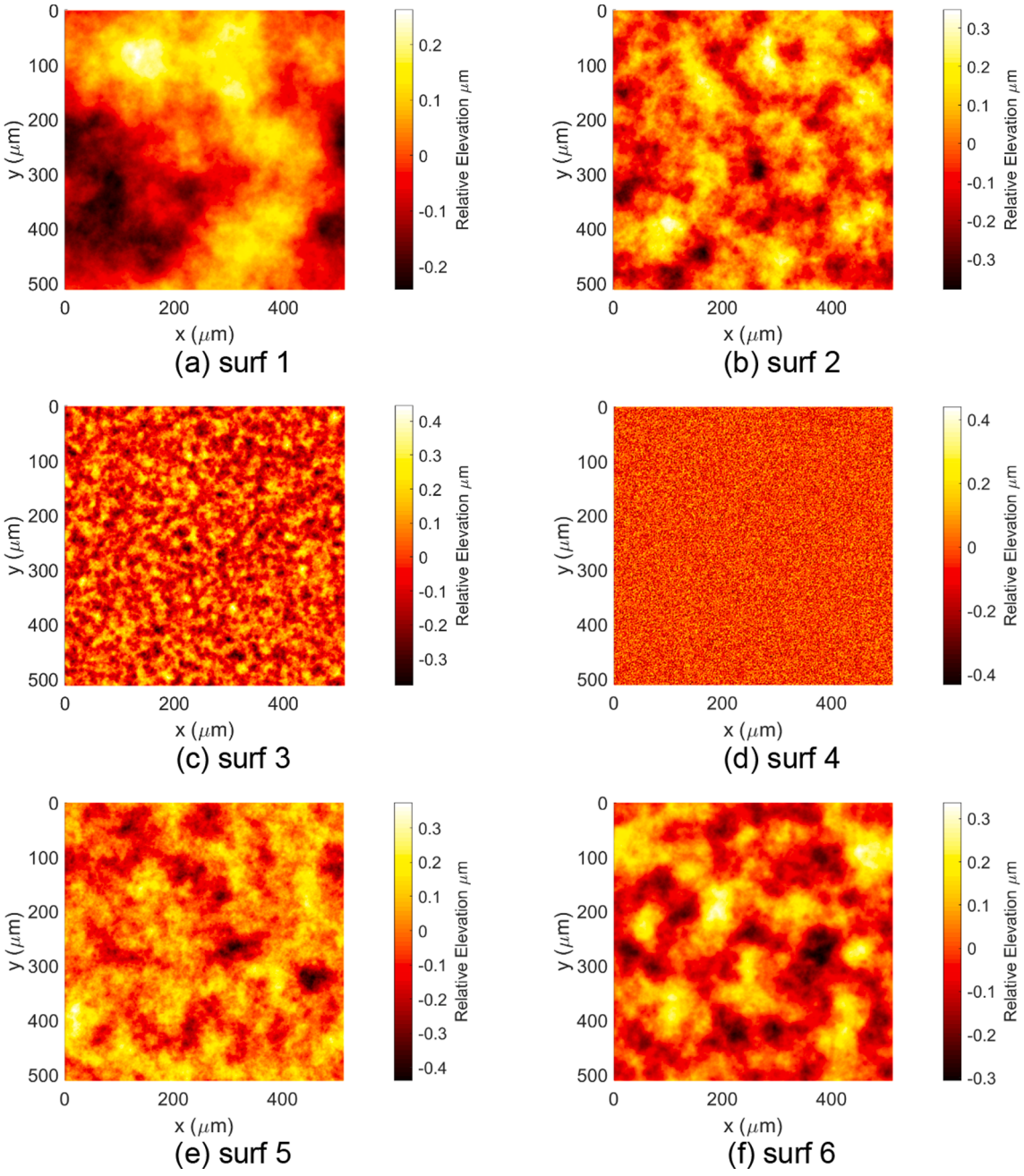


Fig. 6. Topography of computer-generated surfaces used in this study.

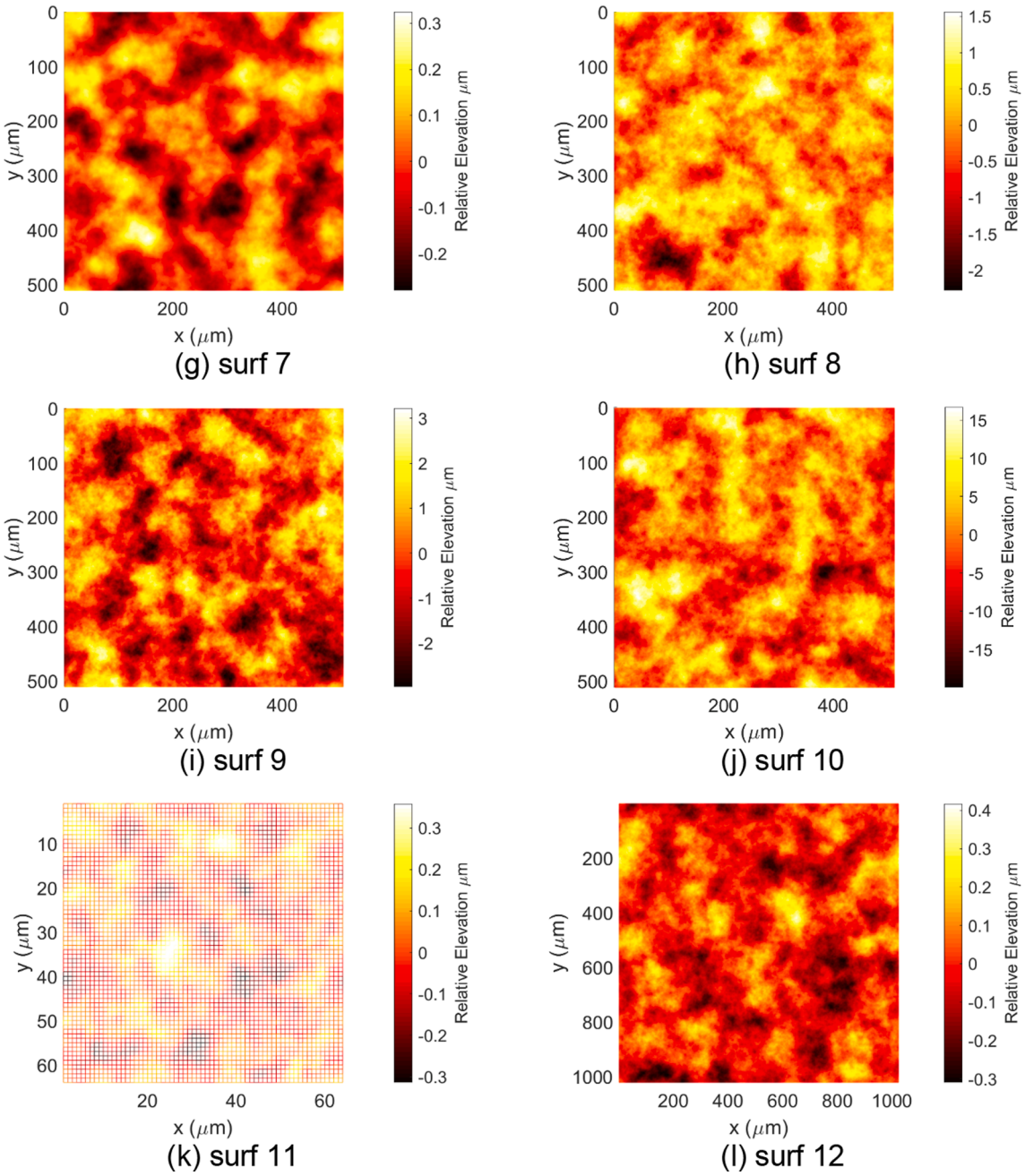


Fig. 6. (*continued*).

adhesion and other dependant properties (see Müser, 2016b; Ciavarella, 2019; Violano et al., 2021).

This work aims to use a state-of-the-art numerical model based on BEM and Fast Fourier Transform (FFT) to test the validity of such analytical models, intending to advance constitutive contact laws in the DEM. The Methodology is explained in the next section, followed by the Results and Discussion.

2. Materials and methods

2.1. Contact mechanics model

The model presented in this work uses an in-house contact mechanics solver previously developed by Ghanbarzadeh et al. (2016). The model incorporates real rough surfaces as numerical inputs along with other material parameters such as Young's modulus (E) and Poisson's ratio (υ). When two rough surfaces are in contact and individual asperities bear the load, the area of contact will be inhomogeneous due to the nature of surface asperity distributions. The contact pressures, in this case, consist of discrete patches. In order to obtain the real contact area and the pressure tensors, the potential energy of the interface should be minimised (Johnson, 1987).

To start with numerical formulation, the quadratic programming approach is applied to find the contact pressure and surface deformation via minimising the total complementary energy using the variational principle. For a normal contact problem of two elastic surfaces, the total complementary energy V^* is expressed as:

$$V^* = U_E^* - \int_\Omega p(u_{z0}^* + u_{z1}^*)d\Omega = U_E^* - \int_\Omega p\overline{u_z^*}d\Omega, \tag{9}$$

where U_E^* is the internal complementary energy of the stressed elastic

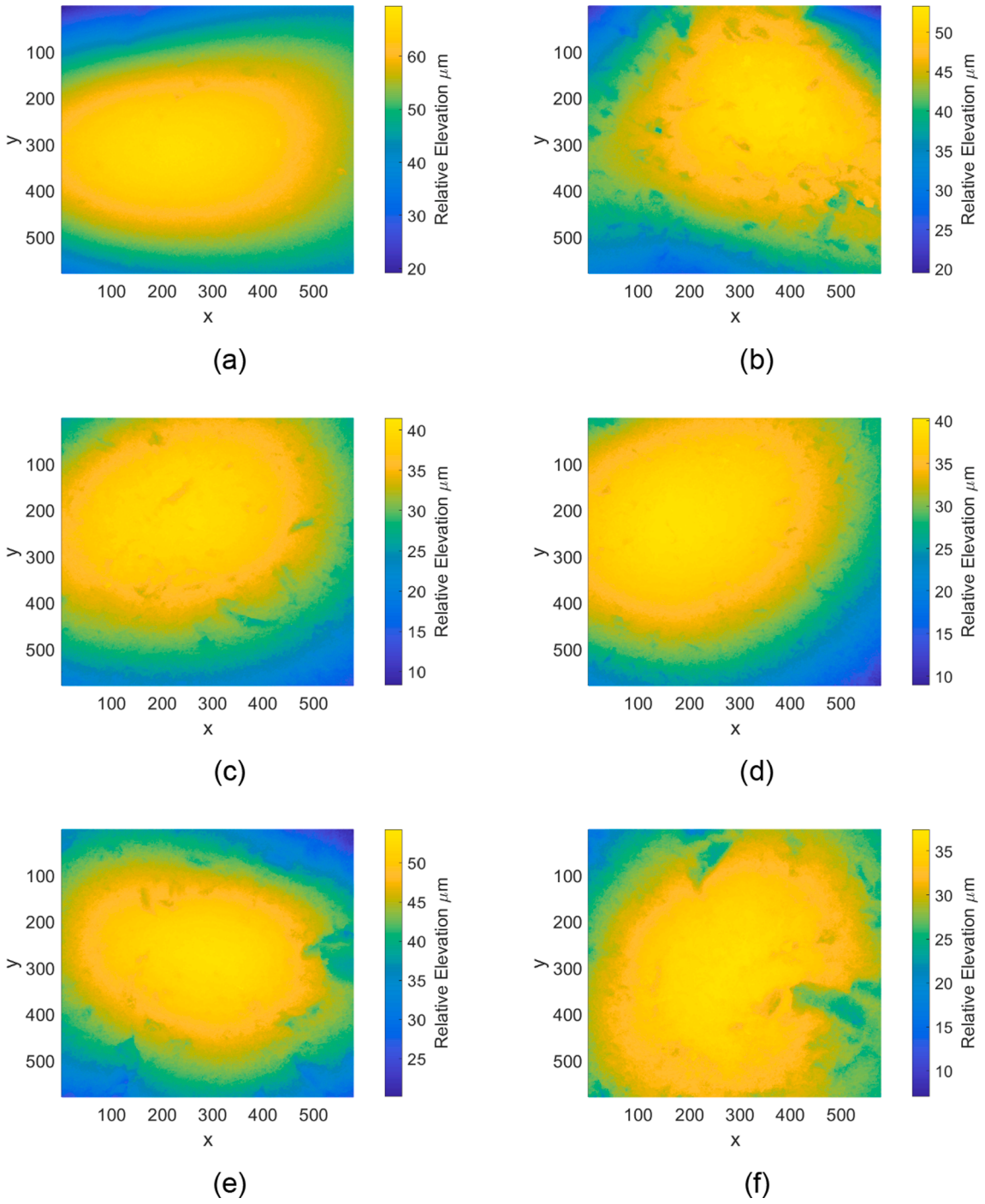


Fig. 7. Topography of rough sand surfaces reported in Yang et al. (2016) for three particle sizes (a),(b) 0.6–1.18 mm; (c),(d) 1.18–2 mm; (e),(f) 2–5 mm (a subset of the 15 analysed surfaces is presented).

solids, Ω is the assumed contacting area where the contact pressure acts, p is the contact pressure, u^*_{z0} and u^*_{z1} are the prescribed displacement of the two contacting solids respectively and $\overline{u^*_z}$ is the total prescribed displacement of the two contacting solids inside the assumed contact domain. Therefore, the term '$\int_\Omega p\overline{u^*_z}d\Omega$' is the work done by the normal force.

For ideal linear elastic materials, the internal complementary energy U^*_E is numerically equal to the elastic strain energy due to the linear relation between the stress and strain as indicated in Fig. 1, which is expressed as:

$$U^*_E = U_E = \frac{1}{2}\int_\Omega p(u_{z0}+u_{z1})d\Omega = \frac{1}{2}\int_\Omega p\overline{u_z}d\Omega \tag{10}$$

where $\overline{u_z}$ is the composite surface displacement inside the contact zone and equals total contact deformation of two contacting solids (denoted as u_{z0} and u_{z1} correspondingly).

To express U^*_E with Eqs. (10) and (9), the complementary potential energy for the normal contact problem is then given by:

$$V^* = \frac{1}{2}\int_\Omega p\overline{u_z}d\Omega - \int_\Omega p\overline{u^*_z}d\Omega \tag{11}$$

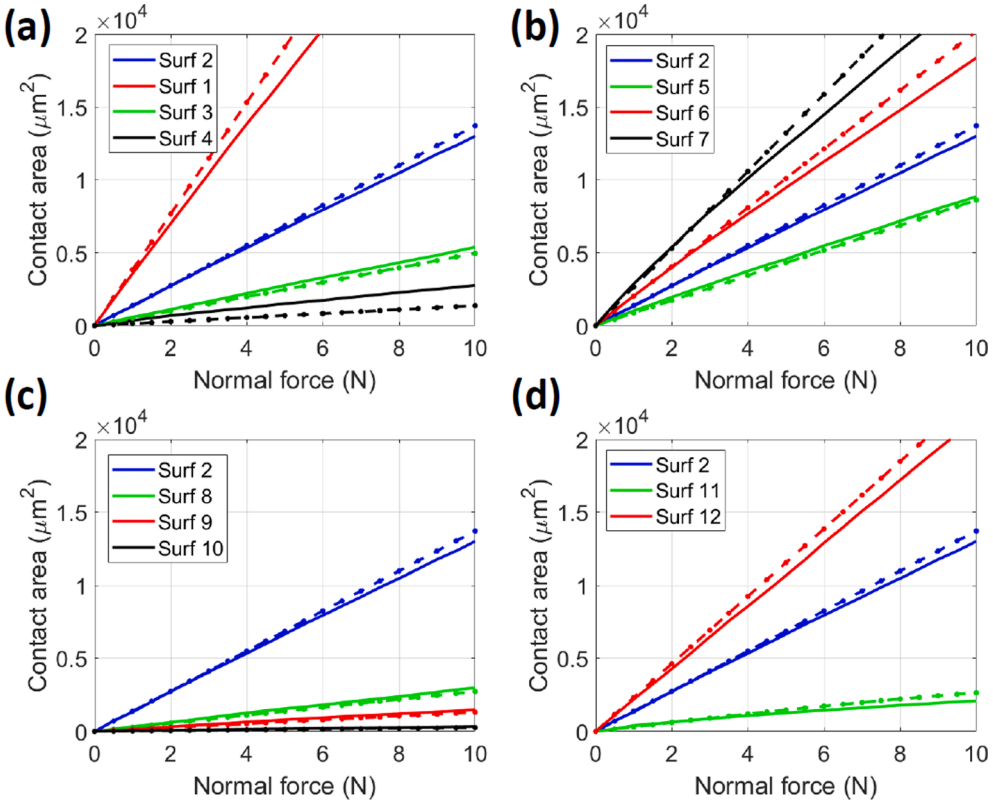


Fig. 8. Prediction of real contact area, for the computer-generated surfaces; solid lines show boundary element estimation, and dashed lines show theoretical estimation of contact area, varying (a) q_0, (b) H, (c) S_q, (d) q_1.

Similarly, the total complementary energy can be minimized for coupled normal and tangential contact problems in the case of linear elastic materials and is expressed as follows:

$$V^* = \frac{1}{2}\int\int t\overline{u}dxdy - \int\int tu^*dxdy, \tag{12}$$

where t is the complete surface stress vector,$\overline{u^*}$ is the prescribed displacement and $\overline{u}$ is the complete surface deformation vector determined by the following equations:

$$t = q_x e_x + q_y e_y + p e_z, \tag{13}$$

$$\overline{u} = u_x e_x + u_y e_y + u_z e_z, \tag{14}$$

where q_x, q_y and p are the traction force, u_x, u_y and u_z are the surface deformation and e_x, e_y and e_z are the Cartesian unit basis vectors in x, y and z directions respectively.

To minimise the complementary potential energy, the contact problem is to find the contact stresses and contact deformations correlated by Eq. (15) which meet a series of restriction conditions. It is noteworthy that after transforming continuous functions into piecewise constant functions that are uniform within the elementary cell of the equally spaced rectangular established in the contact interface, control points for the set grid are necessary. These points are the centroids of each element in the developed model as shown in Fig. 2. Therefore, the shear traction and deformation of each element becomes the focus of the model.

The surface deformations at the interfaces $\overline{u_z}(x,y)$ can be calculated by the discrete convolution of influence matrix and the pressures using the Boussinesq-Cerruti theory (x,y are the lateral coordinates of the surfaces):

$$\overline{u_z} = K^* p_d = \int_{-\infty}^{+\infty}\int_{-\infty}^{+\infty} K(x-\xi, y-\eta)p(\xi,\eta)d\xi d\eta \tag{15}$$

$p(\xi,\eta)$ is the applied load (ξ and η are the coordinates at which the load is applied), K is the convolution kernel and is calculated using half-space approximation:

$$K(x-\xi, y-\eta) = \frac{1}{\pi E^*}\frac{1}{\sqrt{(x-\xi)^2 + (y-\eta)^2}} \tag{16}$$

Moving surfaces in the normal direction will result in interference of surface points and generation of interfacial elastic energy. The gap between surfaces before ($h(x,y)$) and after ($g(x,y)$) the rigid body movement (r) can be formulated as:

$$g(x,y) = h(x,y) + u(x,y) - r \tag{17}$$

Contact pressures $p(x,y)$ at areas where $g(x,y) = 0$ should be positive and zero at areas where $g(x,y)\rangle 0$. The total applied load will be the integration of local pressures at computational elements. The above-mentioned problem can be summarised in the following set of equations:

$$\begin{aligned} &p(x,y)\rangle 0 \qquad g(x,y) = 0 \\ &p(x,y) = 0 \qquad g(x,y)\rangle 0 \\ &\sum_{i,j=1}^{i,j=N} p_{i,j} = F_N \end{aligned} \tag{18}$$

The schematics of the rough surfaces and the interference due to rigid body movement is presented in Fig. 3. Although this approach is applicable to dissimilar materials and tangential loading (Wang et al. 2022), the focus of this study is on the effect of different roughness parameters on the prediction of real contact area for normal contacts.

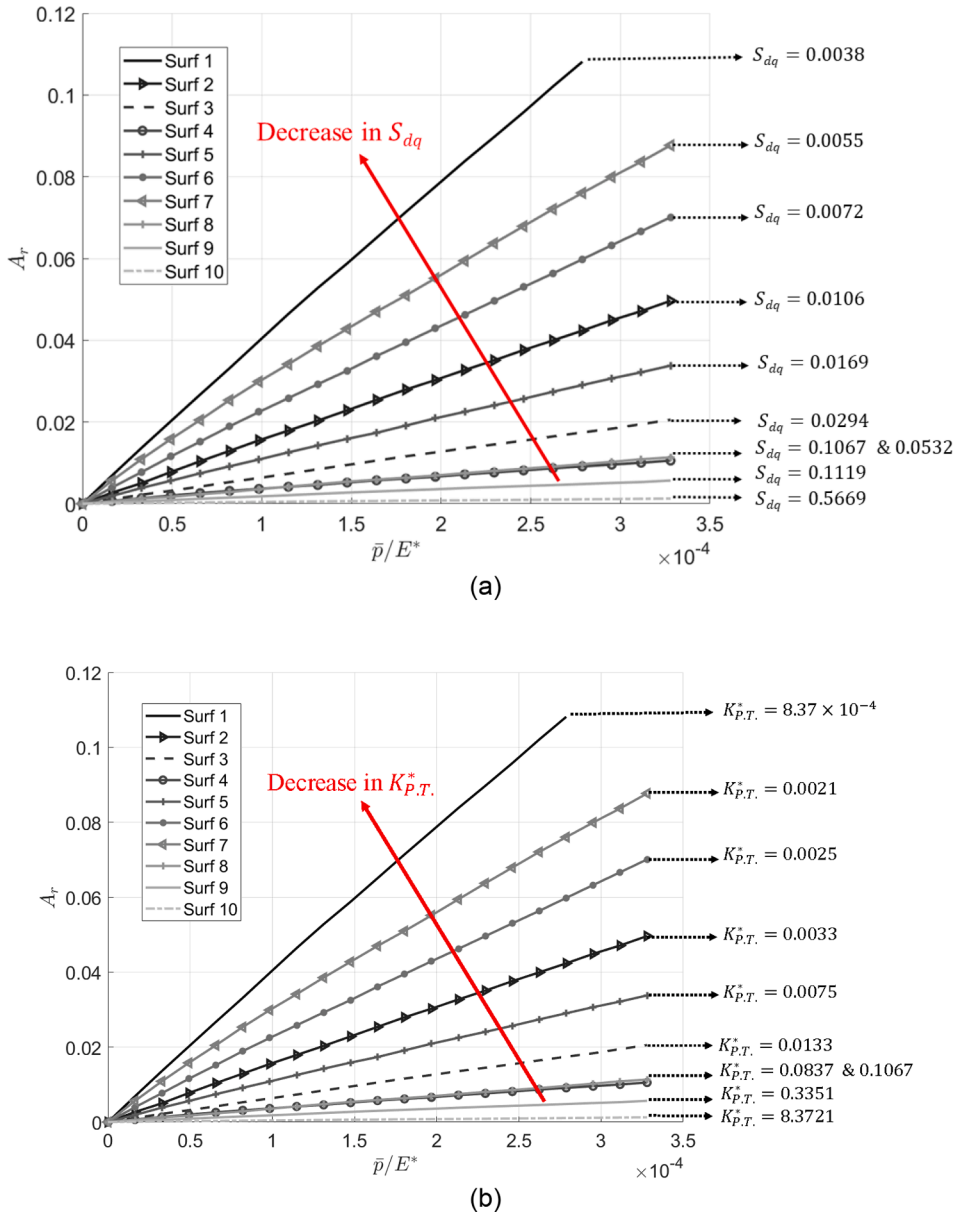


Fig. 9. Relative real contact area A_r (real area of contact over nominal area) versus normalised pressure for numerical simulations of the computer-generated surfaces, (a) with their corresponding values of root mean square gradient of surfaces, (b) with their corresponding values of $K^*_{P.T.} = (S_q^2\, q_0\, H)/(2H\text{-}1)$ expressed in μm.

2.2. Rough surface generation

Here we have generated rough surfaces with self-affine properties to examine the effect of different surface characteristics on the real area of contact for rough surfaces. Surfaces are generated using the Power Spectrum Density (PSD) as reported by Persson (2014). Random numbers were used along with Fourier transforms of the height function ($\tilde{h}(q)$). The height spectrum $C(q)$ was defined as:

$$C(q) = C(q_r) \times \begin{cases} 1 & \lambda_r < \dfrac{2\pi}{q} \le L \\ (q/q_0)^{-2(1+H)} & \lambda_s \le \dfrac{2\pi}{q} < \lambda_r \\ 0 & \end{cases} \tag{19}$$

In which λ_r is the roll-off wavelength, λ_s is the short wavelength cut-off, L is the length of the surface in each dimension, $q_0 = \frac{2\pi}{\lambda_r}$ and H is the Hurst parameter which is calculated by $H = 3 - D_f$ where D_f is the fractal dimension. All the surfaces generated with this method have a mean value of zero.

Digitised rough surfaces are necessary inputs of the contact mechanics simulation. Incorporation of all these surface parameters in a digitised surface needs careful characterisation of the real surfaces for extracting the desired parameters as input to the surface generation models. An example of the surfaces used in the numerical simulation is shown in Fig. 4. The upper surface is set to be perfectly smooth and rigid.

2.3. Prediction of real contact area

Müser (2016) has further developed a theory for the calculation of real area of contact firstly introduced by Pastewka and Robbins (2016) and demonstrated that the model can accurately capture the non-adhesive contact behaviour of rough surfaces. He has introduced a new formula by improving the Pastewka and Robbins criteria using a

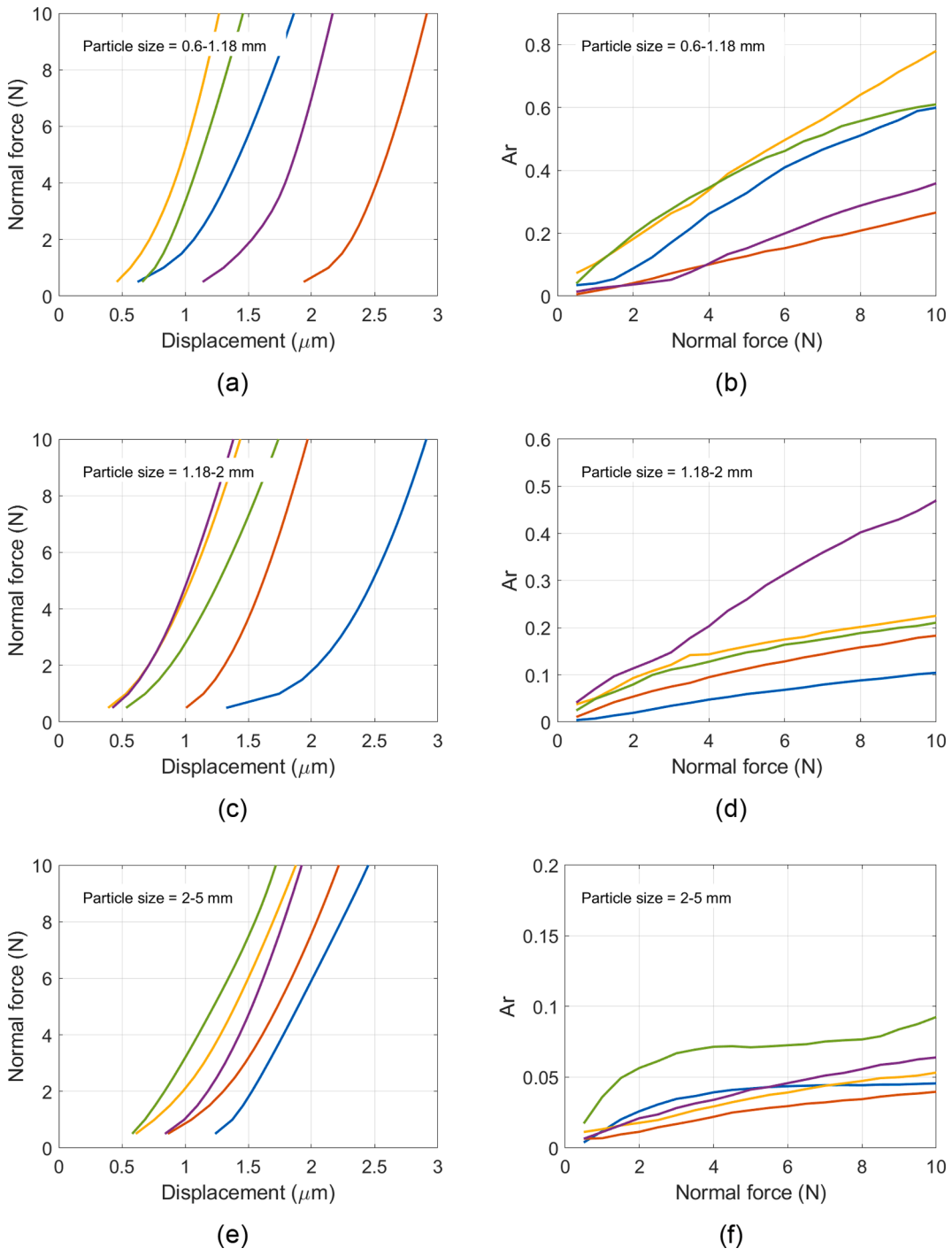


Fig. 10. BEM results of the contact behaviour between the natural sand surfaces and a smooth loading plate. Normal force–displacement and relative contact area-normal force graphs are shown for particles of sizes (a),(b) 0.6–1.18 mm; (c),(d) 1.18–2 mm; (e),(f) 2–5 mm.

new equation by eliminating the mean-field approximation as follows:

$$A_r(k\widetilde{p}) = \pi a_0^2\left(1-\frac{1}{2k^2\widetilde{p}^2}\right)\mathrm{erf}(k\widetilde{p})+\frac{\exp\left(-k^2\widetilde{p}^2\right)}{\sqrt{\pi}k\widetilde{p}} \tag{20}$$

In Eq. (14), A_r is the relative real contact area, k is a constant that is often equal to 2 for real engineering surfaces, $\widetilde{p}$ is calculated by $\widetilde{p}=\frac{3F_N}{4\sqrt{\pi}E^*S_{dq}a_0^2}$ and represents the average contact pressures; and a_0 is the radius of the nominal contact area. Eq. (6) theoretically represents the dependence of the real area of contact on S_{dq} which is calculated using the following equation:

$$S_{dq}^2 = 2\pi\int_{q_0}^{q_1} q^3C(q)dq \tag{21}$$

where q_0 and q_1 are the short and long wavevectors, respectively. Fig. 5 shows the schematic representation of the S_{dq}.

In parallel attempts, Persson and Tosatti (2001), Ciavarella (2019) and Violano et al. (2021) have developed theories for the stickiness of surfaces in adhesive contacts of fractal surfaces. Based on their arguments, the stickiness criterion is the following:

$$S_q < \sqrt{\beta\lambda_r I_a} \tag{22}$$

in which β is a constant that is different for each of the reported works (β $\frac{2H-1}{H}$), and I_a is (w_0/E^*). This criterion suggests that only S_q and the large wavelength (short wavevector) of roughness are responsible for stickiness. Based on this and rearranging Eq. (16), we will suggest a formula that accounts for all these surface parameters excluding material parameters (w_0/E^*) which we call $K_{P.T}$ descibed by the equation:

$$K_{P.T} = \frac{S_q^2 q_0 H}{2H-1} \tag{23}$$

This parameter ($K_{P.T}$) is a dimensional surface parameter expressed in length units (*e.g.* μm). We have investigated the effect of this parameter on the real area of contact for computer-generated surfaces and surfaces of real sand particles.

2.4. Computer-generated surfaces

We have numerically generated fractal rough surfaces with different characteristics in order to check the above criteria of Eqs. (15) and (17). These surfaces are generated systematically, for varying values of S_q, S_{dq}, q_0, q_1 and H and the effect of each parameter on the real area of contact is presented, along with comparisons with the theories discussed above.

Table 1 presents the summary of parameters for the 12 artificial surfaces generated in this study. Fig. 6 shows the topographical view of these surfaces. To manipulate the q_1 parameter, the surface size is changed. The size of the first 10 surfaces is 512 × 512 data points; for surface 11 it is 64 × 64, and for surface 12 it is 1024 × 1024 (surfaces 11 and 12 represent different q_1 values).

2.5. Natural sand surface roughness

In addition to the computer-generated surfaces where the surface characteristics are methodically controlled, 15 natural sand surface roughness topographies reported in Yang et al. (2016) are simulated using the BEM to quantify their mechanical behaviour and explore the challenges associated with natural surfaces. The material parameters for these surfaces are considered equal to the ones used for the artificially generated surfaces above. The topography for a representative subset of these surfaces is presented in Fig. 7. These surfaces correspond to sand particles of three sizes: 0.6–1.18 mm, 1.18–2 mm and 2–5 mm. Their characteristics are comprehensively reported in their original paper. The results of numerical simulations in terms of force–displacement and relative contact area-normal force are reported in this paper.

3. Results and discussion

The contact mechanics community has not reached a consensus in the search for a comprehensive model that considers the complex nature of surface roughness in predicting the real area of contact. Such a prediction will enable robust calculations of contact pressures and load–displacement curves, which can inform mechanistic models in many areas involving contacting surfaces, such as DEM simulations. In this section, we first investigate two recently proposed models of contact area predictions *i.e.* Pastewka-Robbins and Persson-Tosatti, which do not solely rely on S_q to represent surface roughness. We then test the validity and sensitivity of the model parameters they consider.

3.1. Simulations using computer-generated surfaces

The surfaces, reported in Fig. 6 and Table 1, have been subjected to incremental normal loading up to 10 N. The contact area versus normal force curves are presented in Fig. 8. The solid lines show numerical estimations, while the dashed lines represent theoretical prediction using Eq. (6). In Fig. 8(a), q0 is varying from $2\pi \times 10^4$ to $256\pi \times 10^4$ m^{-1}. It can be seen by increasing q_0 and keeping S_q, H, and q_1 constant, the contact area decreases. Fig. 8(b) shows the results of surfaces with varying H (from 0.6 to 1.2) and constant S_q, q_0 and q_1. Decreasing H led to a decreasing trend in contact area. Fig. 8(c) reports the results of surfaces with constant q_0, H and q_1 and varying S_q from 0.1 to 5 μm. A dramatic change in contact area can be observed by increasing S_q. Finally, Fig. 8 (d) represents a case where q_1 is varied from $0.64\pi \times 10^4$ to $10.24\pi \times 10^4$ m^{-1} and all other parameters are constant. Increasing q_1 led to an increase in contact area.

Results for the first 10 simulations are replotted in Fig. 9 in terms of relative real contact area A_r (*i.e.* real area of contact over nominal area of contact) versus normalised pressure (as mentioned earlier, Surfaces 11 and 12 are different in size, so they are not included in Fig. 9). In Fig. 9 (a), the value of S_{dq} is listed for each surface. A clear trend can be seen of an increasing contact area with decreasing S_{dq}. However, the difference between Surfaces 4 and 8 is minimal.

Fig. 9(b) shows the results with their corresponding values of $K_{P.T}$. An increase in $K_{P.T}$ has led to larger contact area. Although both $K_{P.T}$ and S_{dq} can capture this trend, $K_{P.T}$ values (changing from 8.37×10^{-4} to 8.37 μm) demonestrate a wider range compared to S_{dq} (varying from 0.0038 to 0.5669). This feature can be used to differentiate among a larger variety of surfaces. It must be noted that $K_{P.T}$ is a dimensional number (taking units of length) similar to other surface parameters, such as the root mean square height S_q. Thus, controlling K_{PT} will result in controlling the real area of contact. The maximum value of A_r reported in Fig. 9 is similar to the experimental investigation of Ren et al. (2021).

3.2. Simulations using natural sand surfaces

The simulation results of natural sand surfaces are presented in Fig. 10, where they are categorised based on their particle sizes. Each subfigure shows the results of 5 different cases for each particle size. The observed normal force – displacement behaviour is Hertzian-like in all cases, with varying initial level of plasticity depending on surface roughness. More information on the effect of surface roughness on initial plasticity can be found in Nadimi et al. (2019a). The relative contact area is calculated for each simulation assuming the nominal area is Hertzian for spheres with same diameters as the analysed particles. The mechanical behaviour of these simulations demonstrates similar trends. Two cases stand out corresponding to Fig. 10(d) and 10(f) as their response diverges from the rest. The peak of the surface shown in Fig. 10 (d) is located near the edge of the imaged region of interest, creating a mismatch between the real and the nominal contact area which assumes circular contact area. The surface displayed in Fig. 10(f) exhibits two large features of concavity which results in complex contact behaviour.

Natural particles feature complex surfaces across various scales of observation, which affect their contact characteristics with neighbouring particles. Combined effects of roughness-roundness and roughness-form are possible, depending on the size of the region of interest. In this study, the modelling of the real sand surfaces illustrated in Fig. 7 reveals a combined contribution of roughness and larger morphological features, with the effect of the latter being more prominent for higher levels of displacement as indicated by the Hertzian-like behaviour shown in Fig. 10. Another source of ambiguity could be attributed to the lack of information regarding the exact particle size used to calculate the nominal contact area. Recently, Li et al. (2021) proposed a methodology to decouple surface roughness from form and roundness as an alternative to the method used previously in Yang et al. (2016). The separate contributions of roughness and form can be quantified by combining the methodologies proposed in this study and in Li et al. (2021).

This study focused on the study of normal contact behaviour. The introduction of tangential loads for dissimilar materials will add another level of complexity to the problem. The focus would mainly be on the determination of the areas in stick and slip regions in the contact of dissimilar materials. Additionally, the ploughing mechanism may alter the way roughness comes into play in understanding the interaction of particles.

4. Concluding remarks

Numerical methods such as the BEM code adopted in this paper are ideal for studying the contact behaviour of deterministic rough surfaces and has been used widely in tribology for different applications. A systematic study of the effect of surface roughness on contact behaviour was reported, using parametrically computer-generated surfaces with controlled roughness characteristics. It was shown that both theories proposed by Persson-Tosatti and Pastewka-Robbins can capture the behaviour of fractal rough surfaces under compression. A parameter proposed in this study, $K_{P,T}$, which is based on S_q, q_0 and H, is more sensitive to demonstrate the change in contact area comparing with S_{dq}. The $K_{P,T}$ parameter is considered an improvement compared to traditional parameters (S_q, S_{dq}) used to characterise rough surfaces as it takes to account both the height and the slope of the asperities. Finding the real contact area for a given contact pressure, will enable better estimation of contact forces, such as adhesion, compression, and friction, and the susceptibility to fragmentation, which can be utilised to inform advanced contact laws in the DEM.

Real surfaces reported by Yang et al. (2016) were simulated using the BEM to explore the applicability of the method to natural sands. It becomes evident that the results of natural surfaces are affected by both features of form and surface roughness. In most cases, the natural surfaces showed similar trends as observed from computer-generated surfaces, when the contact area was normalised by the nominal contact area. The assumption made to calculate the nominal contact area based on an equivalent sphere can be improved in future studies. Additionally, considering the effect of geological history on particle form and roughness can provide additional insights toward understanding the contact behaviour of rough particles.

CRediT authorship contribution statement

Sadegh Nadimi: Conceptualization, Methodology, Funding acquisition, Formal analysis, Software, Writing – original draft, Writing - review & editing. **Vasileios Angelidakis:** Formal analysis, Investigation, Visualization, Writing - review & editing. **Masahide Otsubo:** Investigation, Funding acquisition, Writing - review & editin. **Ali Ghanbarzadeh:** Investigation, Resources, Software, Writing - review & editing.

Declaration of Competing Interest

The authors declare that they have no known competing financial interests or personal relationships that could have appeared to influence the work reported in this paper.

Acknowledgment

This work was supported by the Engineering and Physical Sciences Research Council (grant number EP/V053655/1) as a part of 'RAILSANDING' New Investigator Award. The collaboration between Newcastle University and the University of Tokyo was supported by the Japan Society for the Promotion of Science (reference number JPJSBP120195701) and the UK Royal Society (reference number IEC \R3\183026).

References

Afferrante, L., Ciavarella, M., Demelio, G., 2015. Adhesive contact of the Weierstrass profile. Proc. R. Soc. A: Math. Phys. Eng. Sci. 471 (2182), 20150248.
Beheshti, A., Khonsari, M.M., 2012. Asperity micro-contact models as applied to the deformation of rough line contact. Tribol. Int. 52, 61–74.
Cavarretta, I., Coop, M.R., O'Sullivan, C., 2010. The influence of particle characteristics on the behaviour of coarse grained soils. Géotechnique 60 (6), 413–423.
Ciavarella, M., 2020. Universal features in "stickiness" criteria for soft adhesion with rough surfaces. Tribol. Int. 146, 106031.
Ciavarella, M., 2019. A comment on "A dimensionless measure for adhesion and effects of the range of adhesion in contacts of nominally flat surfaces" by MH Müser. arXiv preprint arXiv:1907.06450.
Ciavarella, M., Papangelo, A., 2018. A modified form of Pastewka-Robbins criterion for adhesion. J. Adhes. 94 (2), 155–165.
Feng, Y.T., Zhao, T., Kato, J., Zhou, W., 2017. Towards stochastic discrete element modelling of spherical particles with surface roughness: A normal interaction law. Comput. Methods Appl. Mech. Eng. 315, 247–272.
Ghanbarzadeh, A., Salehi, F.M., Bryant, M., Neville, A., 2019. Modelling the evolution of electrochemical current in potentiostatic condition using an asperity-scale model of tribocorrosion. Biotribology 17, 19–29.
Ghanbarzadeh, A., Wilson, M., Morina, A., Dowson, D., Neville, A., 2016. Development of a new mechano-chemical model in boundary lubrication. Tribol. Int. 93, 573–582.
Greenwood, J.A., Williamsoon, J.B.P., 1966. Contact of nominally flat surfaces. Proc. R. Soc. Lond. Ser.-A1966; 295:300–19.
Greenwood, J.A., Tripp, J.H., 1967. The elastic contact of rough spheres. Trans. ASME. J. Appl. Mech. 34 (1), 153–159.
Hanaor, D.A., Gan, Y., Einav, I., 2013. Effects of surface structure deformation on static friction at fractal interfaces. Géotechnique Letters 3 (2), 52–58.
Hanaor, D.A., Gan, Y., Einav, I., 2016. Static friction at fractal interfaces. Tribol. Int. 93, 229–238.
Johnson, K.L., 1987. Contact Mechanics. Cambridge University Press.
Landolt, D., Mischler, S., Stemp, M., 2001. Electrochemical methods in tribocorrosion: a critical appraisal. Electrochim. Acta 46 (24–25), 3913–3929.
Li, Y., Otsubo, M., Kuwano, R., Nadimi, S., 2021. Quantitative evaluation of surface roughness for granular materials using Gaussian filter method. Powder Technol. 388, 251–260.
Ma, C.C., Zhao, Y., Yam, C.Y., Chen, G., Jiang, Q., 2005. A tribological study of double-walled and triple-walled carbon nanotube oscillators. Nanotechnology 16 (8), 1253.
Magel, E.E., Kalousek, J., 2002. The application of contact mechanics to rail profile design and rail grinding. Wear 253 (1–2), 308–316.
Mollon, G., Quacquarelli, A., Andò, E., Viggiani, G., 2020. Can friction replace roughness in the numerical simulation of granular materials? Granular Matter 22 (2), 1–16.
Moreno-Atanasio, R., Xu, B.H., Ghadiri, M., 2007. Computer simulation of the effect of contact stiffness and adhesion on the fluidization behaviour of powders. Chem. Eng. Sci. 62 (1–2), 184–194.
Müser, M.H., Dapp, W.B., Bugnicourt, R., Sainsot, P., Lesaffre, N., Lubrecht, T.A., Persson, B.N., Harris, K., Bennett, A., Schulze, K., Rohde, S., 2017. Meeting the contact-mechanics challenge. Tribol. Lett. 65 (118), 1–18.
Müser, M.H., 2016a. On the contact area of nominally flat hertzian contacts. Tribol. Lett. 64 (14), 1–5.
Müser, M.H., 2016b. A dimensionless measure for adhesion and effects of the range of adhesion in contacts of nominally flat surfaces. Tribol. Int. 100, 41–47.
Nadimi, S., Otsubo, M., Fonseca, J., O'Sullivan, C., 2019a. Numerical modelling of rough particle contacts subject to normal and tangential loading. Granular Matter 21 (4), 1–14.
Nadimi, S., Ghanbarzadeh, A., Neville, A., Ghadiri, M., 2019b. Effect of particle roughness on the bulk deformation using coupled boundary element and discrete element methods. Comput. Particle Mech. 7, 603–613.
Otsubo, M., O'Sullivan, C., Sim, W.W., Ibraim, E., 2015. Quantitative assessment of the influence of surface roughness on soil stiffness. Géotechnique 65 (8), 694–700.
Otsubo, M., O'Sullivan, C., Hanley, K.J., Sim, W.W., 2017. The influence of particle surface roughness on elastic stiffness and dynamic response. Géotechnique 67 (5), 452–459.
Otsubo, M., O'Sullivan, C., 2018. Experimental and DEM assessment of the stress-dependency of surface roughness effects on shear modulus. Soils Found. 58 (3), 602–614.
Pastewka, L., Robbins, M.O., 2016. Contact area of rough spheres: Large scale simulations and simple scaling laws. Appl. Phys. Lett. 108 (22), 221601.
Persson, B.N.J., 2014. On the fractal dimension of rough surfaces. Tribol. Lett. 54 (1), 99–106.
Persson, B.N.J., Tosatti, E., 2001. The effect of surface roughness on the adhesion of elastic solids. J. Chem. Phys. 115 (12), 5597–5610.
Persson, B.N., 2001. Theory of rubber friction and contact mechanics. J. Chem. Phys. 115 (8), 3840–3861.
Ren, J., He, H., Lau, K.C., Senetakis, K., 2021. Influence of iron oxide coating on the tribological behavior of sand grain contacts. Acta Geotechnica 1–23. https://doi.org/10.1007/s11440-021-01367-7.
Sandeep, C.S., He, H., Senetakis, K., 2018. An experimental micromechanical study of sand grain contacts behavior from different geological environments. Eng. Geol. 246, 176–186.
Sandeep, C.S., Li, S., Senetakis, K., 2021. Scale and surface morphology effects on the micromechanical contact behavior of granular materials. Tribol. Int. 159, 106929.
Santamarina, C., Cascante, G., 1998. Effect of surface roughness on wave propagation parameters. Géotechnique 48 (1), 129–136.
Sun, T., Sun, Y., Zhang, H., 2018. Phospholipid-coated mesoporous silica nanoparticles acting as lubricating drug nanocarriers. Polymers 10 (5), 513.
Violano, G., Afferrante, L., Papangelo, A., Ciavarella, M., 2021. On stickiness of multiscale randomly rough surfaces. J. Adhes. 97 (6), 509–527.
Wilson, R., Dini, D., Van Wachem, B., 2017. The influence of surface roughness and adhesion on particle rolling. Powder Technol. 312, 321–333.
Wang, D.D., Boer, G., Nadimi, S., Neville, A., Ghanbarzadeh, A., 2022. A fully coupled normal and tangential contact model to investigate the effect of surface roughness on the partial slip of dissimilar elastic materials. Tribol. Lett. TRIL-D-22-00261.
Wong, C.P.Y., Coop, M.R., 2020. Development of inter-particle friction in a railway ballast. Géotech. Lett. 10 (4), 535–541.

Xiao, H., Liu, S., Wang, D., 2016. Tribological properties of sliding shale rock–alumina contact in hydraulic fracturing. Tribol. Lett. 62 (2), 20.
Yimsiri, S., Soga, K., 2000. Micromechanics-based stress–strain behaviour of soils at small strains. Géotechnique 50 (5), 559–571.
Yang, H.W., Lourenço, S.D., Baudet, B.A., 2022. 3D fractal analysis of multi-scale morphology of sand particles with μCT and interferometer. Géotechnique 72 (1), 20–33.
Yang, H., Baudet, B.A., Yao, T., 2016. Characterization of the surface roughness of sand particles using an advanced fractal approach. Proc. R. Soc. A: Math. Phys. Eng. Sci. 472 (2194), 20160524.
Yao, T., Baudet, B.A. and Lourenco, S.D.N., 2021. Evolution of surface roughness of single sand grain with normal loading, Géotechnique (Ahead of Print). https://doi.org/10.1680/jgeot.20.P.310.
Zhang, N., Ciantia, M.O., Arroyo, M., Gens, A., 2021. A contact model for rough crushable sand. Soils Found. 61 (3), 798–814.